

# UNIVERSITY *of* York

This is a repository copy of *Growth and Crystallisation of Ferromagnetic and Antiferromagnetic Fe<sub>2+x</sub>VyAl Heusler Alloy Films*.

White Rose Research Online URL for this paper:  
<https://eprints.whiterose.ac.uk/132606/>

Version: Published Version

---

## Article:

Huminiuc, Teodor, Whear, Oliver Samuel, Takahashi, Tomoyuki et al. (5 more authors) (2018) Growth and Crystallisation of Ferromagnetic and Antiferromagnetic Fe<sub>2+x</sub>VyAl Heusler Alloy Films. *Journal of Physics D: Applied Physics*. 325003. ISSN 1361-6463

<https://doi.org/10.1088/1361-6463/aacf4c>

---

## Reuse

This article is distributed under the terms of the Creative Commons Attribution (CC BY) licence. This licence allows you to distribute, remix, tweak, and build upon the work, even commercially, as long as you credit the authors for the original work. More information and the full terms of the licence here:

<https://creativecommons.org/licenses/>

## Takedown

If you consider content in White Rose Research Online to be in breach of UK law, please notify us by emailing [eprints@whiterose.ac.uk](mailto:eprints@whiterose.ac.uk) including the URL of the record and the reason for the withdrawal request.



[eprints@whiterose.ac.uk](mailto:eprints@whiterose.ac.uk)  
<https://eprints.whiterose.ac.uk/>

PAPER • OPEN ACCESS

## Growth and characterisation of ferromagnetic and antiferromagnetic $\text{Fe}_{2+x}\text{V}_y\text{Al}$ Heusler alloy films

To cite this article: Teodor Huminiuc *et al* 2018 *J. Phys. D: Appl. Phys.* **51** 325003

View the [article online](#) for updates and enhancements.

### Related content

- [Development of antiferromagnetic Heusler alloys for the replacement of iridium as a critically raw material](#)  
Atsufumi Hirohata, Teodor Huminiuc, John Sinclair *et al.*
- [Large Tunneling Magnetoresistance at Room Temperature Using a Heusler Alloy with the B2 Structure](#)  
Koichiro Inomata, Susumu Okamura, Ryota Goto *et al.*
- [Large tunnel magnetoresistance in magnetic tunnel junctions](#)  
M Oogane, Y Sakuraba, J Nakata *et al.*





**IOP | ebooks™**

Bringing you innovative digital publishing with leading voices to create your essential collection of books in STEM research.

Start exploring the collection - download the first chapter of every title for free.

# Growth and characterisation of ferromagnetic and antiferromagnetic $\text{Fe}_{2+x}\text{V}_y\text{Al}$ Heusler alloy films

Teodor Humeniuc<sup>1</sup>, Oliver Whear<sup>1</sup>, Tomoyuki Takahashi<sup>2</sup>, Jun-young Kim<sup>1</sup>, Andrew Vick<sup>1</sup>, Gonzalo Vallejo-Fernandez<sup>1</sup>, Kevin O'Grady<sup>1</sup> and Atsufumi Hirohata<sup>3,4</sup>

<sup>1</sup> Department of Physics, University of York, Heslington, York YO10 5DD, United Kingdom

<sup>2</sup> Department of Materials Science and Technology, Nagaoka University of Technology, Nagaoka 940-2188, Japan

<sup>3</sup> Department of Electronic Engineering, University of York, Heslington, York YO10 5DD, United Kingdom

E-mail: [atsufumi.hirohata@york.ac.uk](mailto:atsufumi.hirohata@york.ac.uk)

Received 3 January 2018, revised 14 June 2018

Accepted for publication 27 June 2018

Published 13 July 2018



## Abstract

We investigated growth, annealing conditions and magnetic properties of the Heusler alloy  $\text{Fe}_{2+x}\text{V}_y\text{Al}$  by means of x-ray diffraction, magnetic hysteresis and exchange-bias measurements. Ferromagnetic Heusler alloy films were obtained by sputtering  $\text{Fe}_2\text{VAl}$  and  $\text{Fe}_3\text{VAl}$  targets and performing post-growth annealing. The characteristic (220) Heusler alloy peaks were seen in the x-ray diffraction measurements and corresponding ferromagnetic behaviours were observed. In addition, antiferromagnetic Heusler alloy films were deposited by employing Al pegs on  $\text{Fe}_3\text{VAl}$  sputtering targets. The deposited films had elemental ratios close to the predicted  $\text{Fe}_{2.5}\text{V}_{0.5}\text{Al}$  phase, and a 16 Oe exchange-bias was measured in a  $\text{Fe}_{2.3}\text{V}_{0.7}\text{Al}/\text{Co}_{60}\text{Fe}_{40}$  system at 100 K.

Keywords: Heusler alloys, spintronics, sputtering, x-ray diffraction,  $\text{Fe}_2\text{VAl}$ , antiferromagnet, exchange bias

(Some figures may appear in colour only in the online journal)


## 1. Introduction

Antiferromagnetism has been studied both theoretically and experimentally especially over the last few decades since the discovery of giant magnetoresistance (GMR) [1]. Shull and Smart first reported an antiparallel alignment of Mn magnetic moments in MnO [2] which was induced by the superexchange interaction [3] via O atoms. Antiferromagnetic (AF) materials were then found to shift the magnetisation loop of a neighbouring ferromagnetic (FM) material. The shift induced by the

AF in the direction of the applied magnetic field is caused by the exchange coupling induced at the interface between the AF and the FM [4]. This shift has been used to pin the magnetisation of FM thin films and the effect has been implemented extensively in spin valve structures [5]. Recently, AF thin films were found to induce a spin-polarised electrical current [6].

For the majority of commercial spintronic devices, the most commonly used AF material is an Ir-Mn alloy which shows increased magnetic pinning capabilities and corrosion resistance even when the layer thickness drops below 10 nm. However, Ir is one of the scarcest metals in Earth's upper crust and hence an alternative AF material needs to be developed [7]. A significant effort has been devoted to synthesise novel AF Heusler alloys, such as  $\text{Pt}_2\text{MnGa}$  [8],  $\text{Ni}_2\text{MnAl}$  [9] and  $\text{Mn}_2\text{VSi}$  [10], as well as compensated ferrimagnets, e.g.  $\text{Mn}_{2.4}\text{Pt}_{0.6}\text{Ga}$  [11].

<sup>4</sup> Author to whom any correspondence should be addressed.

 Original content from this work may be used under the terms of the [Creative Commons Attribution 3.0 licence](https://creativecommons.org/licenses/by/3.0/). Any further distribution of this work must maintain attribution to the author(s) and the title of the work, journal citation and DOI.

There are over 2500 known possible Heusler alloys, hence identifying possible stable AF candidate constitutes a great challenge [7]. For the  $\text{Fe}_2\text{VAI}$  Heusler alloy, several inconsistencies are observed in the measurements and the predictions of transport and magnetic properties. Nishino *et al* [12] performed temperature dependent resistivity and photoemission spectroscopy measurements and associated the results with the response of a non-magnetic narrow gap semiconductor. A heavy-fermionic behaviour with weak magnetic ordering was observed at temperatures as low as 2K for off-stoichiometric compositions. Popiel *et al* [13] showed that the magnetic properties of  $\text{Fe}_2\text{VAI}$  depend on the crystal structure whereupon  $A2$  structure is FM but the  $B2$  structure is superparamagnetic down to 4.2K. Venkatesh *et al* [14] supported this by performing *ab initio* calculations of  $L2_1$ -ordered  $\text{Fe}_2\text{VAI}$  where several types of disorder were considered for the unit cell. The calculations were then compared to magnetic measurements of  $DO_3$ -type  $\text{Fe}_2\text{VAI}$  which provided further evidence for the magnetic properties being dependent on the atomic disorder in the lattice sites. However, the results point towards paramagnetic and weak magnetic ground states. A schematic representation of the most common type of atomic ordering in Heusler alloys is shown in figure 1 where the Heusler alloy has the general formula  $X_2YZ$ .

Singh and Mazin [15] have predicted a metastable AF state of  $\text{Fe}_2\text{VAI}$  when the compound is iron-rich to become  $\text{Fe}_{2.5}\text{V}_{0.5}\text{Al}$ . Their calculations considered a supercell that was created by quadrupling the  $L2_1$  structure along the (1 1 1) axis. The nearest neighbours of each atom were consistent with the  $B2$  disorder allowing for Fe and V atoms to be easily interchanged. The AF ground state was found by tuning the composition of  $\text{Fe}_{2+x}\text{V}_{1-x}\text{Al}$ . A speculation of AF phases existing in  $\text{Fe}_2\text{VAI}$  was discussed by Feng *et al* [16] as a result of a lower than expected superparamagnetic response observed. To our knowledge, there is no clear evidence that  $\text{Fe}_2\text{VAI}$  would have a stable AF phase. It is expected however that combinations of AF and FM phases might form in polycrystalline samples as previously reported for  $\text{Ni}_2\text{MnAl}$  [17].

A very close relative of  $\text{Fe}_2\text{VAI}$ ,  $\text{Fe}_2\text{VSi}$  was reported to have a stable AF tetragonal ground state at low temperature [18–20]. Fukatani *et al* used this material in a thin-film form deposited on  $\text{MgO}$  and  $\text{MgAl}_2\text{O}_4$  to prove the effects of biaxial strains on the magnetic and transport properties of the Heusler alloy [21]. The results showed an increase of more than 50% of the Néel temperature with a maximum value of 193 K as determined by temperature dependent resistivity measurements.

The key parameter in the AF order is the spacing between planes where the magnetic spins are ordered ferromagnetically in the plane. For  $\text{Fe}_2\text{VAI}$ , the lattice constant is theoretically reported to be 0.576 nm and the AF order is predicted to appear at  $\text{Fe}_{2.5}\text{V}_{0.5}\text{Al}$ . Hence, it is critical to control the composition and the crystallisation processes.

## 2. Experimental procedures

$\text{Fe}_2\text{VAI}$  films were deposited on  $\text{Si}/\text{SiO}_2$  substrates using a PlasmaQuest high target-utilisation sputtering system

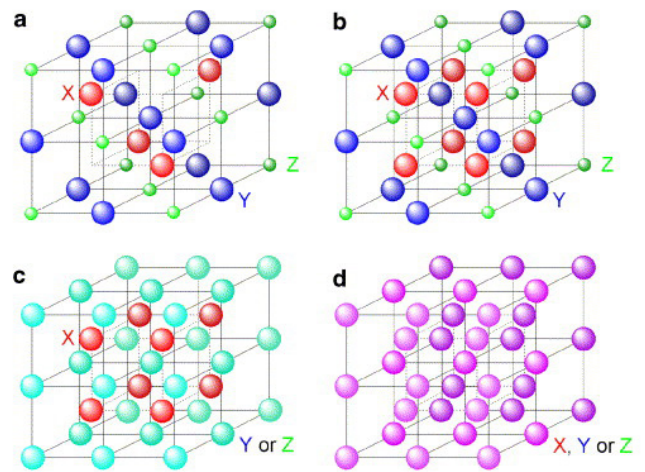


**Figure 1.** Crystalline ordering of Heusler alloys: (a) half-Heusler alloy with the  $C1b$  phase and full-Heusler alloy with the (b)  $L2_1$ , (c)  $B2$  and (d)  $A2$  phases [7]. Reprinted from [7], Copyright 2006, with permission from Elsevier.

(HiTUS) with a base pressure of  $6 \times 10^{-8}$  mTorr. A 13.56 MHz radiofrequency (RF) antenna ionises the process gas (Ar) kept at a constant pressure of 1.86 mTorr. A bias voltage ( $V_B$ ) applied to the target was varied from  $-300$  V to  $-900$  V in order to control the sputtering rate ( $0.2\text{--}0.7 \text{ \AA s}^{-1}$ ) and the grain size of the film. The thickness of the Heusler alloy films was kept constant at 100 nm. A 5 nm-thick capping layer of Ta was used in order to prevent oxidation. The films were post-annealed in a vacuum furnace at a base pressure lower than  $5 \times 10^{-8}$  mTorr.

After each annealing step, magnetisation curves were measured using an alternating gradient force magnetometer (AGFM, Princeton Measurements Model 2900) at room temperature (RT). The exchange-bias measurements were performed using an ADE Model 10 vector VSM equipped with an open cycle cryostat. The crystalline structures were characterised using x-ray diffraction (XRD, Rigaku SmartLab) using a standard collimated beam and a  $\text{Ge}(220)$  2-bounce monochromator optics.

Furthermore, compositions of the sputtered  $\text{Fe}_2\text{VAI}$  films were characterised by inductively-coupled plasma optical emission spectroscopy (ICP-OES) and energy-dispersive x-ray spectroscopy (EDX). The chemical composition analysis by ICP-OES was performed by InterTek Ltd. For the ICP-OES measurements, samples consisted of 100 nm-thick films were deposited on glass substrates. The samples were then dissolved in aqua regia ( $\text{HCl}$ : 15 ml,  $\text{HNO}_3$ : 5 ml) and diluted to a final volume of 30 ml with demineralised water. The solutions were then analysed by ICP-OES while blank glass substrates were also analysed for unexpected contaminants. The EDX analysis was performed using a Thermo Scientific EDX unit attached to FEI Sirion S-FEG/JEOL 7800F Prime scanning electron microscopes.

## 3. Results and discussion

The as-deposited  $\text{Fe}_2\text{VAI}$  films were characterised by XRD. As shown in in figure 2, films deposited at  $-300$  V films showed

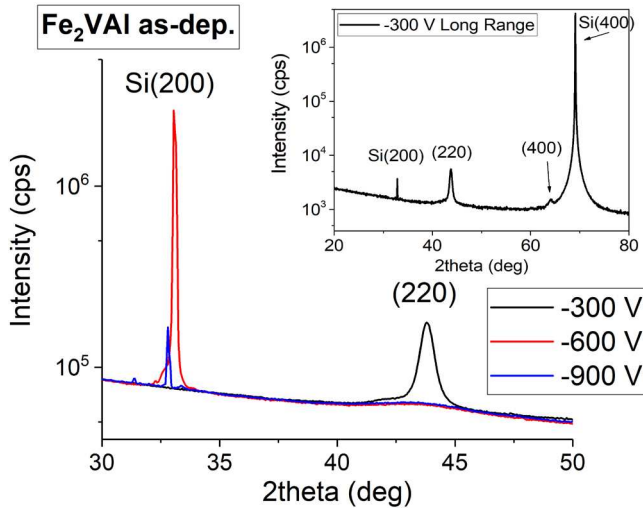


**Figure 2.** XRD data for as-deposited Fe<sub>2</sub>VAI films sputtered at different bias voltage values. The inset shows a longer range XRD scan of the -300 V sample using a Ge(220) × 2 monochromator.

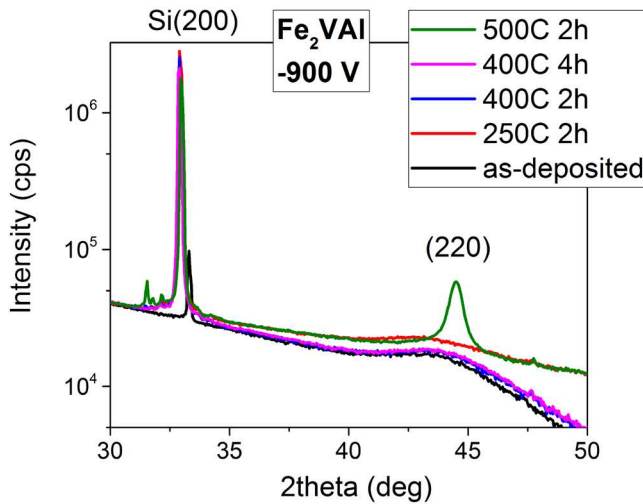


**Figure 3.** XRD data for Fe<sub>2</sub>VAI films deposited at -900 V, post-annealed at increasing temperatures and durations.

a sharp peak at 44.4° which coincided with the Heusler (220) peak position [16]. This structure disappeared when the bias voltage increased to -600 V and -900 V. While the Heusler (200) peaks at ~31° are missing for all samples, a weak (400) Heusler peak at 64° can be seen for the -300 V in a longer range scan in the inset. This suggested the formation of the sought B2 crystalline phase which is predicted to be AF. No (111) family super-lattice peaks corresponding to the fully ordered L<sub>21</sub> phase were visible. Throughout the XRD scans, the forbidden Si (200) reflection can be observed at ~33°. Their appearance and changing intensities were thought to be due to slight misalignments of the samples during sample loadings in the XRD setup.

In order to determine the crystallisation conditions for the alloy deposited at -900 V, a number of samples were annealed under vacuum. As shown in figure 3, the alloy crystallises when annealed at T<sub>a</sub> = 500 °C for 2h. The (220) peak

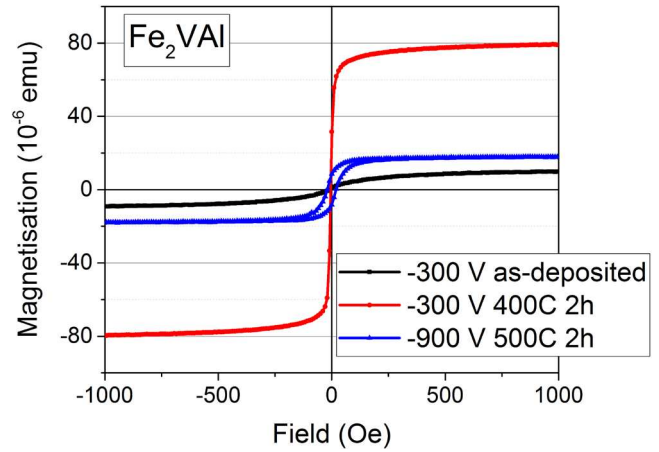


**Figure 4.** Magnetisation curves for Fe<sub>2</sub>VAI films deposited at -300 V and -900 V.

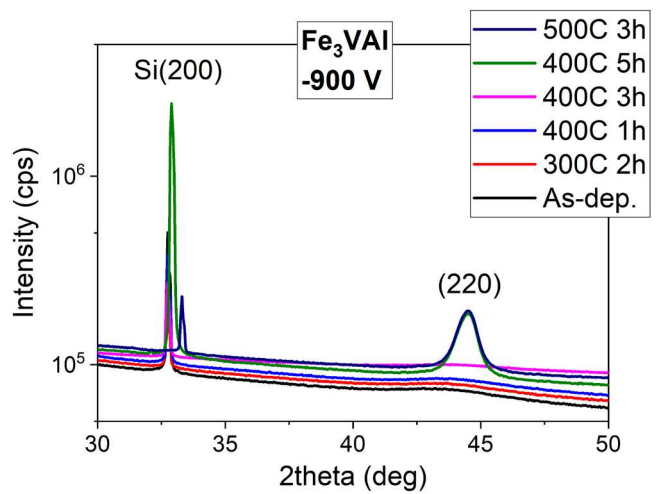


**Figure 5.** XRD data for Fe<sub>3</sub>VAI films deposited at -900 V and post annealed at increasing temperatures and durations. For better representations, y-offsets of 5000 counts-per-second were applied for each XRD scans.

indicates a strong A2 type structure. The absence of the (200) peak indicated a lack of the higher-ordered B2 phase.

By performing Scherrer analysis [22], the mean grain sizes of these two sets of films were found to be similar, i.e. 14.8 ± 0.7 nm for those sputtered at -300 V and 14.3 ± 0.8 nm for Fe<sub>2</sub>VAI sputtered at -900 V and post-annealed. This was different when compared to our previous report on the crystallisation of the FM Co<sub>2</sub>FeSi Heusler alloy [9]. We conclude that the grain size control during the deposition had little influence on the crystallisation process for the Fe<sub>2</sub>VAI films.

As shown in figure 4, the FM behaviour in Fe<sub>2</sub>VAI films sputtered at -300 V and -900 V could be a consequence of formation of A2 Heusler structure as predicted [15]. It is clear that the stoichiometric alloy has a tendency to crystallise in a FM phase. The AF phase is predicted to form when an off-stoichiometric Fe-rich composition is achieved. The chemical composition analysis by ICP-OES on the -300 V and -900 V films provided Fe:V:Al composition ratios of 55.25:16.53:28.22 and 53.75:20.09:26.16, respectively, with

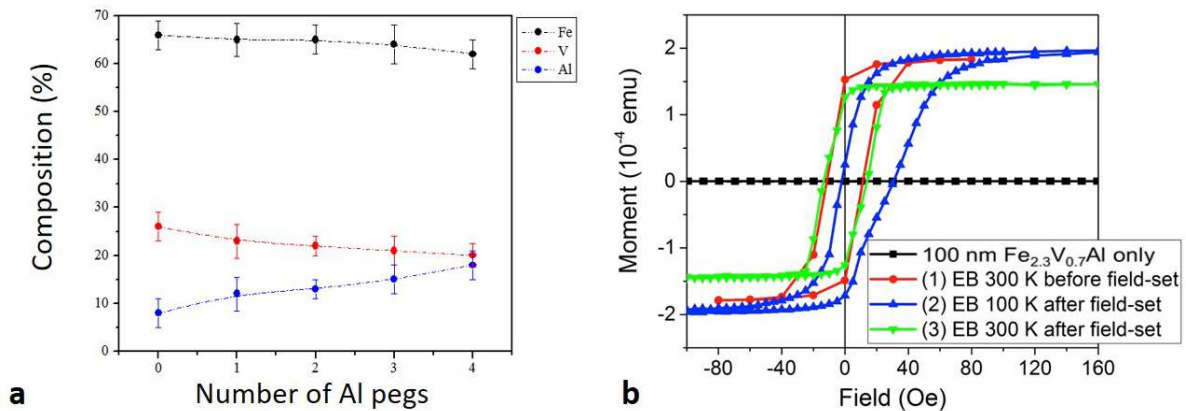


**Figure 6.** (a) Atomic composition of the doped Fe<sub>3</sub>VAl films with different number of 6 mm diameter Al pegs. (b)  $M$ - $H$  curves of a 100 nm-thick Fe<sub>2.3</sub>V<sub>0.7</sub>Al films and a Fe<sub>2.3</sub>V<sub>0.7</sub>Al/Co<sub>60</sub>Fe<sub>40</sub> exchange-bias stack before and after the field annealing.

errors of  $\pm 0.01$ . This suggested elemental compositions of Fe<sub>2.0</sub>V<sub>0.6</sub>Al and Fe<sub>2.1</sub>V<sub>0.8</sub>Al for the films deposited at  $-300$  V and  $-900$  V, respectively. Both compositions pointed to Fe deficiencies and V surpluses when compared to the target composition of 2.5:0.5:1.

To achieve the desired AF composition of Fe<sub>2.5</sub>V<sub>0.5</sub>Al, a more Fe-rich Fe<sub>3</sub>VAl target was used. As-deposited films were found to have a composition of Fe<sub>2.6</sub>VAl<sub>0.4</sub> by ICP-OES. From the XRD measurements, the Heusler alloy (220) peaks are observed for the samples annealed at 400 °C for 5 h and at 500 °C for 3 h (see figure 5). Temperatures between 400 °C and 500 °C were found to be the minimum temperatures for the A2 crystallisation to occur in these films.

The as-deposited Fe<sub>3</sub>VAl samples were measured to have the element ratio of 2.5:1:0.3 using the more Fe-rich Fe<sub>3</sub>VAl target. In order to increase the Al content to reach the predicted 2.5:0.5:1 AF ratio [7], high-purity Al pegs (6 mm in diameter) were placed on top of the Fe<sub>3</sub>VAl target during sputtering. As shown in figure 6(a), it was possible to increase the Al content of the films with increasing numbers of Al pegs. A composition ratio close to 3:1:1 was achieved. With further processes of sputtering with Al pegs, we obtained films with a composition ratio of 2.3:0.7:1, close to the AF composition of Fe<sub>2.5</sub>V<sub>0.5</sub>Al, as observed by EDX method.

Magnetic properties of a 100 nm-thick Fe<sub>2.3</sub>V<sub>0.7</sub>Al films were measured as seen in figure 6(b). Compared to the Fe<sub>2.3</sub>V<sub>0.7</sub>Al/Co<sub>60</sub>Fe<sub>40</sub> stacks, the magnetic response of the Fe<sub>2.3</sub>V<sub>0.7</sub>Al layer was very weak. This suggested that the exchange-shifted FM signals were from the CoFe layer itself and its interaction with the non-magnetic/AF Heusler alloy layer.

The exchange-bias stack structure consisted of Si/SiO<sub>2</sub> substrate/5 nm Cr/30 nm Ag/20 nm Fe<sub>2.3</sub>V<sub>0.7</sub>Al/3 nm Co<sub>60</sub>Fe<sub>40</sub>/2 nm Ta. The Cr is used as a smoothing layer for the substrate, the Ag is a well-known seed layer for the Heusler structure and has a good lattice match with the alloy [23]. The sample was then field-annealed at 500 K under  $-2$  T applied field for 90 min, and then cooled to 100 K with the applied field, following the York Protocol [24]. Three  $M$ - $H$  hysteresis curves in figure 6(b) show in sequence: (1) at 300 K before the field annealing, (2) at 100 K field-cooled after the  $-2$  T

field annealing at 500 K, then (3) at 300 K after warming up from the 100 K measurement. A larger coercivity, as well as an exchange-bias of around 16 Oe was observed at 100 K after the field-set, indicating the exchange-bias coupling at the Fe<sub>2.3</sub>V<sub>0.7</sub>Al/Co<sub>60</sub>Fe<sub>40</sub> interface. Due to the small exchange-bias measured, we could not determine the average blocking temperature as similarly reported on Mn<sub>2</sub>VSi [10]. The modest loop shift values and the decreased thermal stability were attributed to the lack of anisotropy associated with the cubic structure. Most cubic Heusler alloys exhibit comparable properties with regards to the pinning strength and thermal stability of the AF configuration of the magnetic moments. In order to increase the thermal stability and pinning strength, a tetragonal distortion of the lattice is required. Further element replacement in the Fe<sub>2</sub>VAl alloy and strain introduction to induce magnetic anisotropy may increase the exchange-bias as well as the blocking temperature for RT antiferromagnetism.

#### 4. Conclusion

A systematic study of structural and magnetic properties was performed on Fe<sub>2+x</sub>V<sub>y</sub>Al layers deposited by sputtering Fe<sub>2</sub>VAl and Fe<sub>3</sub>VAl targets with Al dopant pegs. The FM A2 structure Fe<sub>2</sub>VAl was confirmed by XRD and magnetic measurements for  $-300$  V and  $-900$  V films after annealing at 500 °C for 2 h. By sputtering Fe<sub>3</sub>VAl target with Al pegs, Fe<sub>2.3</sub>V<sub>0.7</sub>Al films were deposited whose elemental ratio was close to the predicted AF Fe<sub>2.5</sub>V<sub>0.5</sub>Al. A very weak magnetic response of a 100 nm-thick Fe<sub>2.3</sub>V<sub>0.7</sub>Al film as well as a 16 Oe exchange-bias shift observed in a Fe<sub>2.3</sub>V<sub>0.7</sub>Al/Co<sub>60</sub>Fe<sub>40</sub> stack suggested AF nature of the Fe<sub>2.3</sub>V<sub>0.7</sub>Al films.

#### Acknowledgment

This work is partially funded by EU-FP7 HAFIR (NMP3-SL-2013-604398) and UK EPSRC (EP/M02458X/1).

#### ORCID iDs

Jun-young Kim  <https://orcid.org/0000-0002-1639-3270>

Gonzalo Vallejo-Fernandez  <https://orcid.org/0000-0002-4826-1547>

Atsufumi Hirohata  <https://orcid.org/0000-0001-9107-2330>

## References

- [1] Baibich M N *et al* 1988 *Phys. Rev. Lett.* **61** 2472–5
- [2] Shull C G and Smart J S 1949 *Phys. Rev.* **76** 1256
- [3] Anderson P W 1950 *Phys. Rev.* **79** 350
- [4] Meiklejoh W H and Bean C P 1957 *Phys. Rev.* **105** 904
- [5] Fontana R E Jr *et al* 1997 *US Patent* 5,701,223
- [6] Jungwirth T, Marti X, Wadley P and Wunderlich J 2016 *Nat. Nanotechnol.* **11** 231
- [7] Hirohata A *et al* 2006 *Curr. Opin. Solid State Mater. Sci.* **10** 93–107
- [8] Singh S, D'Souza S W, Suard E, Chapon L, Senyshyn A, Petricek V, Skourski Y, Nicklas M, Felser C and Chadov S 2016 *Nat. Commun.* **7** 12671
- [9] Tsuchiya T, Kubota T, Sugiyama T, Huminiuc T, Hirohata A and Takanashi K 2016 *J. Phys. D: Appl. Phys.* **49** 235001
- [10] Wu H, Vallejo-Fernandez G and Hirohata A 2017 *J. Phys. D: Appl. Phys.* **50** 375001
- [11] Nayak A K *et al* 2015 *Nat. Mater.* **14** 679
- [12] Nishino Y, Kato M, Asano S, Soda K, Hayasaki M and Mizutani U 1997 *Phys. Rev. Lett.* **79** 1909–12
- [13] Popiel E, Tuszynski M, Zarek W and Rendecki T 1989 *J. Less-Common Met.* **146** 127–35
- [14] Venkatesh C, Srinivas V, Rao V V, Srivastava S K and Babu P S 2013 *J. Alloys Compd.* **577** 417–25
- [15] Singh D J and Mazin I 1998 *Phys. Rev. B* **57** 14352
- [16] Feng Y *et al* 2001 *Phys. Rev. B* **63** 165109
- [17] Acet M, Duman E, Wassermann E F, Mañosa L and Planes A 2002 *J. Appl. Phys.* **92** 3867–71
- [18] Kawakami M, Yamaguchi K and Shinohara T 1999 *J. Phys. Soc. Japan* **68** 2128
- [19] Lue C S, Kuo Y K, Hong S N, Peng S Y and Cheng C 2005 *Phys. Rev. B* **71** 064202
- [20] Endo K, Matsuda H, Ooiwa K and Itoh K 1995 *J. Phys. Soc. Japan* **64** 2329–32
- [21] Fukatani N, Ueda K and Asano H 2011 *J. Appl. Phys.* **109** 073911
- [22] Cullity B D 1977 *Elements of X-Ray Diffraction* (Reading, MA: Addison-Wesley)
- [23] Sagar J *et al* 2012 *IEEE Trans. Magn.* **48** 4006–9
- [24] O'Grady K, Fernandez-Outon L E and Vallejo-Fernandez G 2010 *J. Magn. Magn. Mater.* **322** 883–99